

Photonic Band Gap Aperture Coupled Fractal Shape Tri-Band Active Antenna

Tale Saeidi^{1, *}, Idris B. Ismail¹, Mojtaba Ahadi², and Adam R. H. Alhawari³

Abstract—A modified Koch fractal shape is used to decrease the dimensions of an antenna and resonates at more than one band for agricultural application. A new feeding technique of aperture coupled method called a non-uniform annular Photonic Band Gap is applied in order to integrate the designed antenna to the active elements. Subsequently, a transmission line transformer is designed using Genetic algorithm to achieve a perfect matching between the active element (amplifier) and the load (antenna). The proposed antenna is designed and fabricated. The results show that the proposed antenna has a high gain of 20.5 dB, 21 dB, and 22 dB at 0.915 GHz, 1.8 GHz and 2.45 GHz respectively with a compact size and low cost. The results predict its prospect as a promising alternative to the conventional one, which is compatibly applicable to agriculture applications especially when multiband function is required.

1. INTRODUCTION

Nowadays, the product protection against pest in agriculture becomes a challenging problem, and the cooperation of the scientific fields to solve it is increasing. Therefore, protections of these products before and after harvesting is a great concern. One of the most effective and destructive problems in this matter is protecting them from grain insects. There are many strategies such as applying physical and thermal methods, X-ray, microwave (MW) energy, etc. But among all these techniques, MW energy was a promising way to terminate the insects present in grain products. The most important reasons that forced the scientists to use the MW energy were having no chemical residues in food and thus no side effects on the human body. MW energy also does not have adverse impacts on the environment around. Insects cannot tolerate this treatment and even cannot continue developing [1–3]. Based on the Federal Communications Commission (FCC), the approved frequency bands for this purpose are 47.5 MHz, 915 MHz, 1.8 GHz, and 2.45 GHz. According to [4, 5], microstrip antennas can be utilized at microwave frequencies due to their small size, light weight, thin profile configuration, low fabrication cost, inclination to mass production, etc. [6, 7]. In order to decrease the cost of the antenna caused by its large dimensions, many techniques, such as changing and optimizing the shape of the antenna to enhance the electrical length of the antenna, exploiting a substrate with high permittivity, using reactive or resistive loading, and applying and altering notches or stubs positions on the patch, can be applied as reported in [8]. Furthermore, there are some other ways that can be useful. For instances, the defects in the patch metallization lead to noticeable radiator miniaturization. However, one can observe that such a technique decreases antenna resonant frequency, so antenna optimization is necessary. An integrating approach to antenna miniaturization involves the utilization of metamaterials. However, the use of artificial materials leads to certain fabrication problems, and the design process becomes complex.

Received 29 August 2016, Accepted 21 October 2016, Scheduled 21 November 2016

* Corresponding author: Tale Saeidi (gs32772@gmail.com).

¹ Faculty of Electrical and Electronic Engineering, Universiti Teknologi Petronas, Malaysia. ² Department of Computer and Communication, Faculty of Engineering, University Putra Malaysia, Malaysia. ³ Department of Electrical Engineering, Faculty of Engineering, Najran University, Saudi Arabia.

One of the solutions to above limitations can be reached by means of fractal curves. It has been reported that the application of space filling fractal curves enables us to achieve considerable miniaturization and also wideband and multi-band properties [9,10]. Hence, in order to optimize the shape of patch and not to face the aforementioned problems, a fractal shape can be used which was first introduced in 1975 [11]. Currently, the fractal antenna geometries are widely utilized in many applications such as wireless communication systems due to their compact size, low cost, capability of multi-band operation, ease of feeding, wide bandwidth, multiband and low profile [12,13]. The most common fractal geometries which have been used in antenna designs are the Sierpinski gasket or carpet fractal [14], Hilbert fractal [15], Minkowski [16], Square Curve fractals and Koch fractal [17]. In microwave networks, matching the source and the load to the transmission line or waveguide is necessary for maximum power delivery [18]. Several works have been done to demonstrate different techniques of matching transformers for two arbitrary frequencies [19–21]. The Chebyshev filter, Genetic Algorithm (GA) and Particle Swarm Optimization (PSO) algorithm can be used in order to speed up the solving process and optimize the results easily.

Passive antennas have some drawbacks compared to active antennas in radiating structures, and their gain and bandwidth are less [22]. Active antennas have several advantages such as increasing the effective length of the antenna, enhancing the bandwidth, reducing the mutual coupling between two array elements and improving the noise factor [23]. Active antennas can be made by integrating the passive part with an active element as diodes or transistors [24]. Various interests in wireless communication systems, incompatibility and efficiency have made a fast progress and growth in the microwave and monolithic microwave integrated circuit (MMIC) technologies [25]. As an important building block in wireless systems, low noise amplifier (LNA) can be defined as a receiver's performance. Generally, for designing the LNA, some considerations should be kept in mind, such as optimum input matching, optimum gain, low power consumption, high linearity and low noise figure [26].

In this work, a triple-band active antenna using fractal shape is presented for agriculture applications. A non-uniform annular Photonic Band Gap (PBG) aperture coupled feed method is utilized to integrate the designed antenna to the active elements. Then, GA algorithm is used to match the active element (amplifier) to the load (antenna). Evidently, the proposed method makes the design method for active antennas simpler and more efficient. Finally, a high gain active antenna with high-quality performance is demonstrated.

2. PASSIVE ANTENNA DESIGN

Selecting the substrate material for an active antenna is a crucial factor that should be considered in the antenna design. The substrate selection should be done carefully; a thick substrate with low permittivity for the patch layer to have better radiation efficiency and larger bandwidth and a thin substrate with a high permittivity for the feed line to shrink the undesired radiations and coupling [27,28]. In this work, for radiator patch, four layers of RT Duroid 5880 with dielectric constant of 2.2 and thickness of 0.787 mm is selected and stacked with each other using super glue with $\epsilon_r = 3.3$. Moreover, an FR4 substrate with $\epsilon_r = 4.4$ and a thickness of 1.6 mm as the thinner layer is used for the feed line which is integrated with the LNA circuitry. Four elements of modified Koch fractal shape compounding with a square loop [6] have been applied to reduce the antenna size and function as an antenna at three frequency bands. As illustrated from Fig. 1, the proposed passive antenna includes a Koch fractal shape which has been modified as a patch, and seven shorting pins connect the patch to the ground where the antenna is fed by a 50 Ohm SMA connector. Table 1 indicates the dimensions of the antenna.

Table 1. Passive antenna dimensions.

L_s (mm)	70
L_p (mm)	58.26
W_s (mm)	70
W_p (mm)	58.26
W (mm)	3

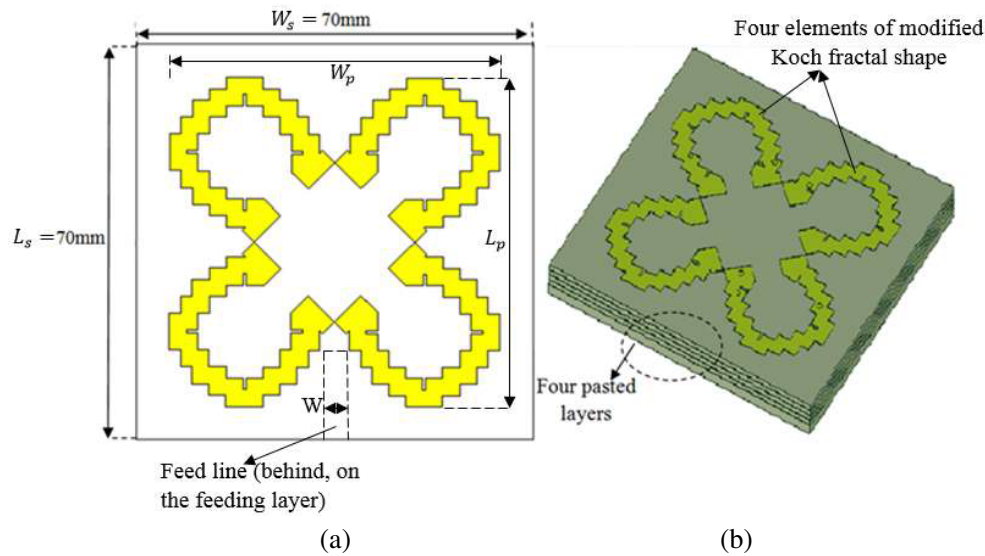


Figure 1. Prototype of the passive antenna, (a) top view and (b) perspective view.

First, a single element of 90-degree modified Koch fractal shape compounding with a circularly polarized (CP) square loop microstrip line (Fig. 2) as a monopole antenna with a half-wave length according to the first resonant frequency (at 0.915 GHz) is designed. The modified Koch fractal is constrained up to the second iteration only. Increment in iterations enhances the small edges mostly, which is practically useless in increasing the electrical length.

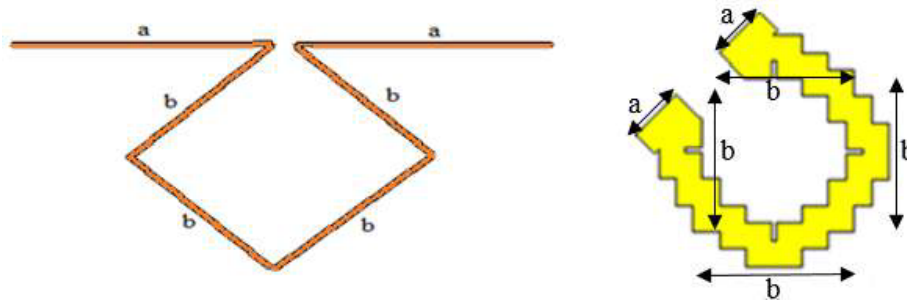


Figure 2. CP square loop microstrip line (a), the proposed modified Koch element compounded with CP square transmission line (b).

Then, to have more than one resonant frequency, the elements of the radiator patch are increased to two, three and four elements. Based on the reasons explained before, a modified 90-degree Koch fractal shape antenna is compounded with the CP square loop microstrip line to decrease the antenna as much as possible.

Afterward, seven shorting pins (via) connect the patch to the PBG which plays as the aperture part of the feeding technique (Aperture Coupled Feeding). The reasons behind using the shorting pins can be seen in the next paragraph. The size of the patch can be reduced by using shorting pins. In addition, for further size reduction, the shorting pins are used as a loading in such a spot (location on the antenna) where the electric field or current density is high at desired frequency. The shorting pins can be located either at the edge or at the corner. For instance, a shorting pin at a corner of the patch gives us a maximum reduction in antenna size. Moreover, applying shorting pins at the edge of the radiating patch can yield a higher loading effects, and the resonant frequency is lower when the shorting pin is located at the edge and corner, thus maximum reduction of the antenna size is achieved at this location of shorting pin. However, a good reduction can be achieved by pin loading, but it reduces the

gain and bandwidth (BW). In spite of the decrement in gain, BW can be compensated by applying compact antenna layers, aperture coupled feeding, etc.

According to surface current intensity around the rings presented in Fig. 3, the shorting pins' positions can be optimized to suppress the surface current intensity, surface waves and fringing fields. Thereafter, a PBG structure is applied as an aperture for aperture coupled feeding technique. Moreover, surface wave as a serious problem in the design of microstrip antenna can be suppressed. When the substrate permittivity $\epsilon_r > 1$, surface waves will be infused on microstrip antennas [29]. Some unfavorable specifications such as end-fire radiation, edge diffraction, and incorrect coupling between different antenna elements caused by surface waves. The aforementioned characteristics of surface waves will create reduction in antenna efficiency, gain, restriction in the BW and raising cross polarization level. Besides, miniaturization of the microstrip antenna and the integrated MW circuits might be hindered due to high permittivity of substrates.

The ground is periodically loaded by three annular rings. Therefore, the surface wave can be suppressed to present a forbidden frequency range (bandgaps or stop band) for the antenna at the operating frequency. Furthermore, the coupled space wave with radiated power and the other destructive effects such as board system interference and mutual coupling between elements will be hindered hereinafter [30, 31].

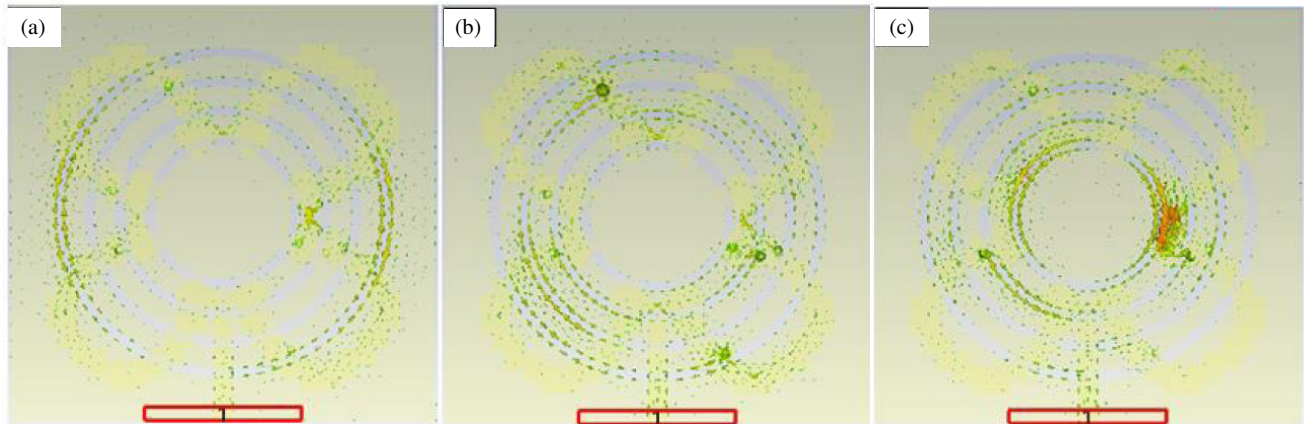


Figure 3. Current distribution around the patch and annular rings.

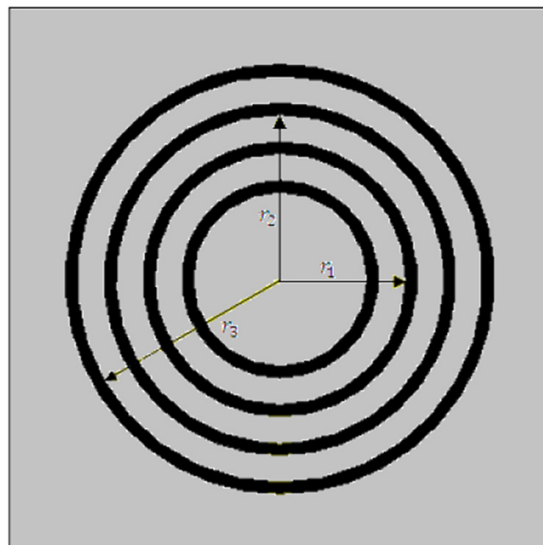


Figure 4. Annular PBG structure.

Three non-uniform ring-shaped patterns are etched from the ground layer with a period of ‘ a ’. Two main parameters that should be well considered to obtain the stopband characteristics are the period ‘ a ’ of the rings as a width of the rings and the filling factor ‘ r/a ’ (r is the radius of the rings). As can be illustrated from the following figure, ‘ a ’ is unchanged, and ‘ r ’ for each ring declines compared to the first ring (first ring for first band operation) [32]. As can be seen in Fig. 4, the first ring (outer ring) is the biggest, and it is related to 0.915 GHz, while the second (middle ring) and third (inner ring) are designed at the frequency of 1.8 GHz and 2.45 GHz, respectively. In accordance to surface current intensity around the rings, the shorting pins’ positions can be optimized to suppress the surface current intensity, surface waves and fringing fields.

3. ACTIVE ANTENNA DESIGN

After the passive antenna performance is designed and the result validated through simulation and measurement, it is tangible that the gain of the designed antenna is low and not applicable for the design purpose. Therefore, in this study, a surfacemount amplifier ‘LEE-39+’ as an active element is used to enhance the gain of the designed antenna. Based on the amplifier’s data sheet [33], this amplifier has an internal impedance equal to 50 and a gain of 22.3, 18.7, 14.7 dB at 0.915, 1.8 and 2.45 GHz, respectively [33]. The real part of the input impedance of the designed passive antenna itself (Z_{11}) at the operating frequency 0.915 GHz is $87\ \Omega$, and it is not matched to the amplifier impedance. Consequently, an impedance matching circuit is presented to transfer the maximum power from the amplifier to the antenna. A three-section transmission line transformer (TLT) matching method is applied to solve this problem (Fig. 5). To get the best and optimized values of every section of TLT from the simulation, two different optimizing methods are exploited apart from the analytical method and Chebyshev filter.

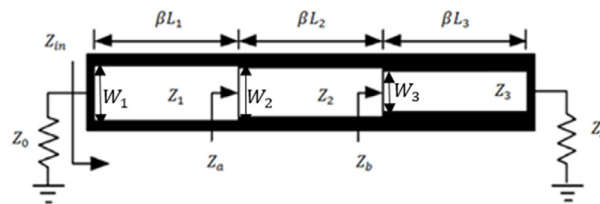


Figure 5. Three sections transmission line transformer [34].

As illustrated in Fig. 5, each section of the 3-section transformer consists of two variables, namely impedance (Z) and electrical length (βL). The analytical method presented in [35] is applied to get the actual values of every section, and then the Chebyshev filter technique reported in [18, 36] is applied for validation purposes. Afterward, two different algorithms are used to optimize the obtained values of the transmission line transformer specifications. First, Particle Swarm Optimization (PSO) algorithm is exploited to obtain the valid variables needed. To use the PSO for a given problem, each member in the swarm is called a particle with assumed number of $M = 50$. The considered members exist in an N -dimensional solution space to alter their positions in accordance to either their last best performance or the other particles’ best previous performance in the swarm. For every member in the N -dimensional problem, two M by N matrixes of a velocity (v) and position (x) are specified [26]. Here, PSO algorithm is performed using the assumed parameters as follows: $M = 50$, $c1 = c2 = 2$, $V_{\max} = (1 + k)/2$ where k is the impedance transformation ratio, $k = Z_A/Z_0$. The stopping standard is that either a fitness (desired) value (in the simulation is considered less than 10^{-6}) or a maximum number of 10,000 iterations is reached. Furthermore, to have the final compact design, the following limitations are defined: less than $\lambda_1/4$ for length of each section which is the wavelength at the first band design frequency. As an initiation for PSO algorithm usage, the impedance and length values are randomly applied with the intervals for impedances between Z_A and Z_0 , and lengths between $\lambda_1/10$ and $\lambda_1/4$, respectively. Moreover, in the simulation process, f_1, f_2, f_3, Z_A, Z_0 are considered constant and equal to 0.915 GHz, 1.8 GHz, 2.45 GHz $87\ \Omega$, $50\ \Omega$, respectively. But the best solution cannot be achieved from the first run, thus, the simulation running continues more than 10 runs to approximately get the desired solution.

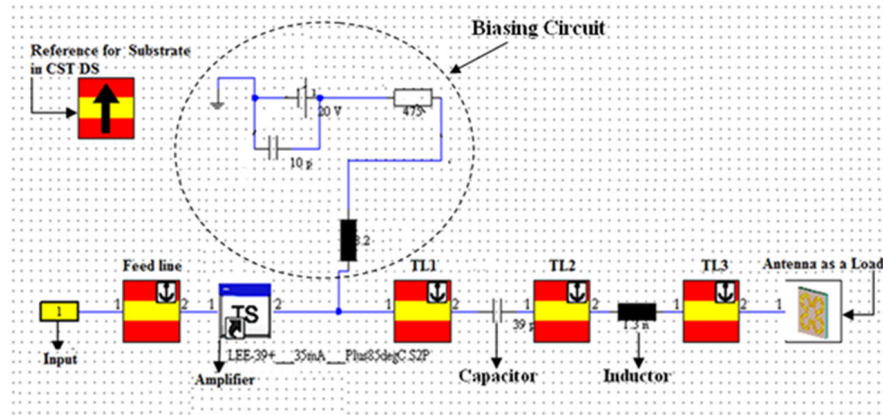


Figure 6. Transmission line transformer circuit in CST design studio.

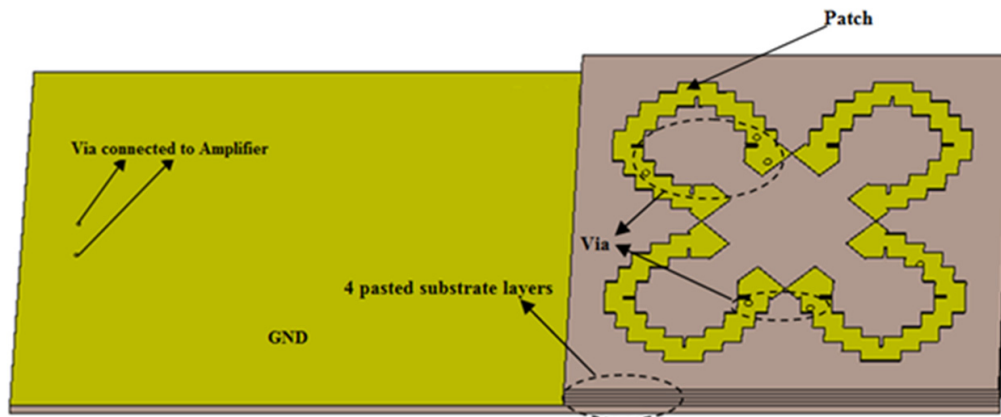


Figure 7. Front view of the proposed active antenna.

The second technique of the optimization is the Genetic Algorithm (GA). The details and required equations are presented in [34, 37]. After achieving the result values from each of the algorithms, the proposed active antenna is implemented using CST Design Studio as illustrated in Fig. 6. Obviously, the GA's outcomes are the best among them because of the perfect matching and less spending time for simulation and running as will be discussed in the next section. In the simulation, each section has the length in degrees, and it can be changed to mm, while the width in mm can be extracted from impedance in Ohm [35].

Subsequently, the simulated results of the modified Koch fractal active antenna and TLT circuit are validated, and the proposed design of TLT is fabricated. As a next step, the feeding layer should be changed to a new one with the TLT matching circuit and the amplifier [28]. These steps of the whole simulation can be seen in Figs. 7 and 8, respectively.

Later, the measurement process is divided into two parts. The first part is to measure the S -parameters, and the second one is to measure the gain of the antenna. For measuring and validating the simulation outcomes, a Vector Network Analyser (model: Anritsu 37347D) with a frequency range of 40 MHz–20 GHz is used. At the beginning of the measurement process, one port calibration method is performed based on partial Thru-Reflect-Line (TRL) with the VNA in accordance to Agilent's standards (short, open and terminator) using calibration kit model 3652. Then, the measured results are compared with the simulated ones. To measure the gain of the antenna, the method presented in [38] is utilized. In each measurement process, the proposed antenna is connected to the transmitter, which is a Signal Generator (model: Anritsu-MG3700A) with the frequency range of 250 KHz–3 GHz, and antenna with a known gain is connected to a receiver, which can be a Spectrum Analyser (model: ADVANTEST R3267) with a frequency range of 100 Hz–8 GHz. The results are presented in the next section.

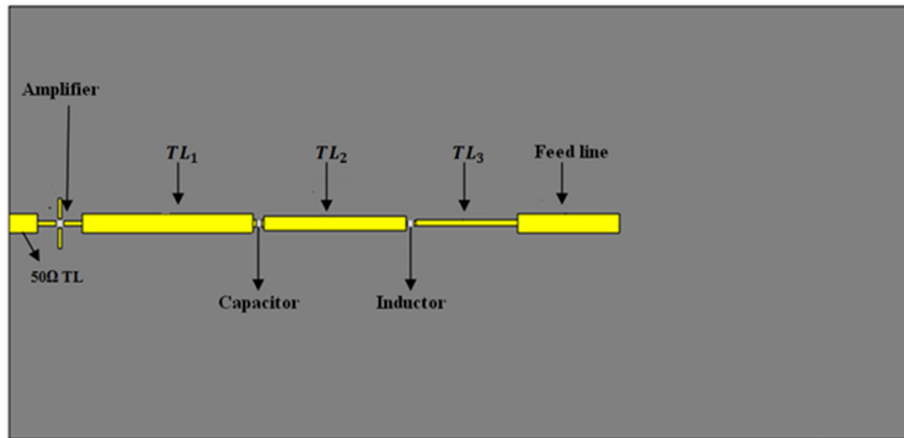


Figure 8. The feeding view of the proposed active antenna with TLT circuit.

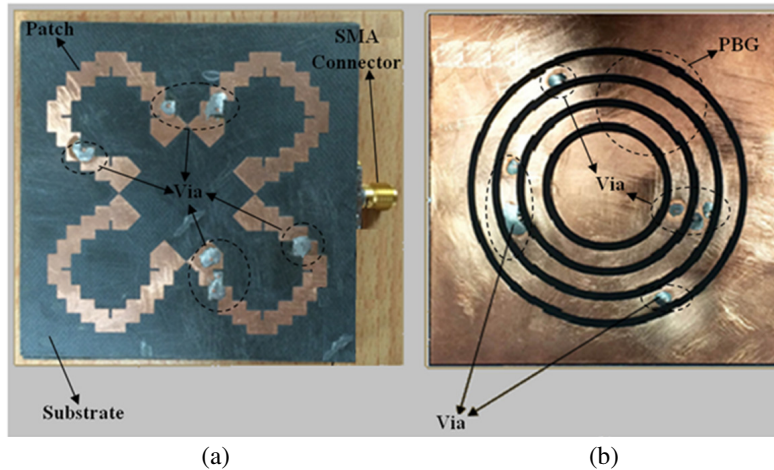


Figure 9. Photograph of the fabricated passive antenna. (a) Top layer and (b) bottom layer.

4. RESULTS AND DISCUSSION

4.1. Passive Antenna

The proposed antenna performances are investigated and simulated using CST simulator in terms of gain, radiation efficiency, and reflection coefficient. After choosing the most applicable feeding type for the antenna, it is integrated with the active component. To achieve this, the substrate thickness of the patch layer should be thicker with less permittivity. Fig. 9 shows photos of the fabricated passive antenna, and its reflection coefficient result is demonstrated in Fig. 10. As can be seen from Fig. 10, the simulation result produces center resonant frequencies at 0.915 GHz, 1.8 GHz, and 2.45 GHz. Meanwhile, the measured result generates the center of resonant frequencies at 0.915 GHz, 1.60 GHz, and 2.20 GHz. It is also depicted that the antenna achieves the resonant frequency between 1.75 GHz and 1.9 GHz with reflection coefficient level of -10 dB. It is shown that there is a small deviation for the second and third resonances with deviations of 0.20 GHz and 0.25 GHz, respectively. The simulated frequency is shifted slightly to higher frequencies. There are two undesired resonances which are pointed with circle marker. These two new harmonics and the frequency shifting occur due to the unwell distribution of the air and the super glue used to paste the layers and fabrication tolerances. The passive antenna's radiation properties are presented in Table 2.

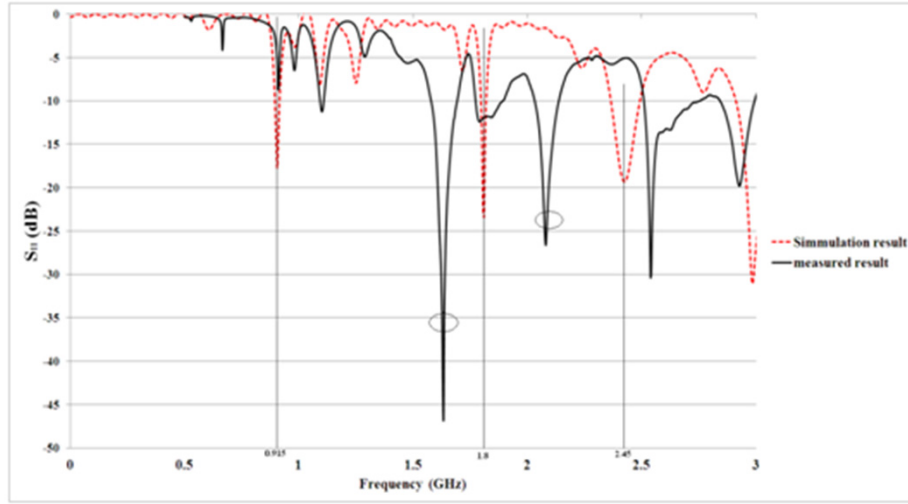


Figure 10. The simulated and measured reflection coefficient results of the passive antenna.

Table 2. Characteristics of the passive antenna.

f_r (GHz)	Radiation Efficiency (%)	Z (Ω)	Gain (dB)	VSWR
0.915	50	87	0.2	1.8
1.8	40	34.5	0.512	1.5
2.45	78.14	66.13	2.52	1.3

Table 3 shows the comparison of the proposed passive antenna with some recent analogous works with respect to the size reduction. The proposed antenna has a miniaturized size almost by 18%, 70%, 30%, 65%, 65%, 12.5%, and 12.5%, respectively.

Table 3. Size reduction comparison between the proposed antenna and previous works.

Antennas	Dimensions (mm) (L \times W)
Proposed design	70 \times 70
[39]	80 \times 86
[40]	92 \times 240
[41]	85 \times 100
[42]	200 (diameter- circle shape)
[43]	200 (diameter-circle shape)
[44]	80 \times 78.93
[45]	80 \times 80

4.2. TLT DESIGN

According to the figures presented in Table 2, the antenna has a good matching impedance where the Voltage Standing Wave Ratio (VSWR) is less than two at 915 MHz, 1.8 and 2.45 GHz. In addition, it has a considerable gain and radiation efficiency. The antenna is bidirectional at the higher frequencies and unidirectional at the lower one. Due to the low gain of this antenna, an active component (amplifier) is

Table 4. TLT dimensions using four different methods.

Method	W_1 (mm)	W_2 (mm)	W_3 (mm)	L_1 (mm)	L_2 (mm)	L_3 (mm)
Analytical	2.517	1.791	1.213	58.500	32.600	58.500
Chebyshev	2.46	1.79	1.24	58.500	58.500	58.500
PSO	2.44	1.78	1.26	37.000	40.000	35.400
GA	2.46	1.799	1.25	40.000	42.000	40.000

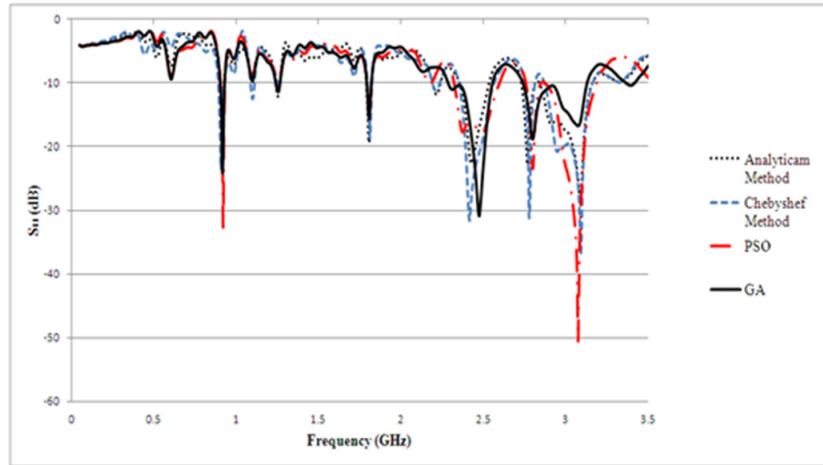


Figure 11. The simulated reflection coefficient result of the proposed active antenna using four different methods of impedance matching.

integrated to the antenna for gain enhancement. Then, four different methods of impedance matching are analysed to effectively match the passive antenna to the amplifier. The dimensions for each part of the TLT are shown in Table 3, while the results of S_{11} , Z_{11} and VSWR at each resonance frequency are presented in Table 4.

As shown in Table 4, after applying all the four methods to TLT to achieve a perfect matching between the amplifier and the antenna, the extracted results from the GA optimization technique demonstrate the best matching results among the other methods. Fig. 11 shows the reflection coefficient simulation result of the proposed active antenna using four different matching methods.

4.3. ACTIVE ANTENNA

The fabricated active antenna prototype with the active element (amplifier) together with the biasing circuit and the TLT is shown in Fig. 12. For comparison purposes, the reflection coefficient results of the proposed active antenna can be demonstrated from Fig. 13, while the simulated and measured gains are presented in Table 5. Good agreement between the simulated and measured results is obtained. As can be shown from Table 5, the output gain of the antenna is totally improved using the amplifier.

As depicted in Fig. 13 for the simulation and measurement result, the active antenna generates center resonant frequencies at 0.915 GHz, 1.8 GHz, and 2.45 GHz (simulation result). Meanwhile, the measurement result illustrates the center of resonant frequencies at 0.878 GHz, 1.78 GHz, 2.40 GHz and 2.61 GHz. It is also depicted that the antenna achieves the acceptable bandwidth between 1.5 GHz and 1.9 GHz and the range from 2.20 GHz to 2.75 GHz with reflection coefficient level less than -10 dB. Furthermore, it is shown that there is a deflection for the third resonance with deviation of 0.160 GHz. There are two undesired resonances which are pointed with circle marker in passive reflection coefficient's figure. These two new harmonics and the frequency shifting which occur due to the unwell distribution

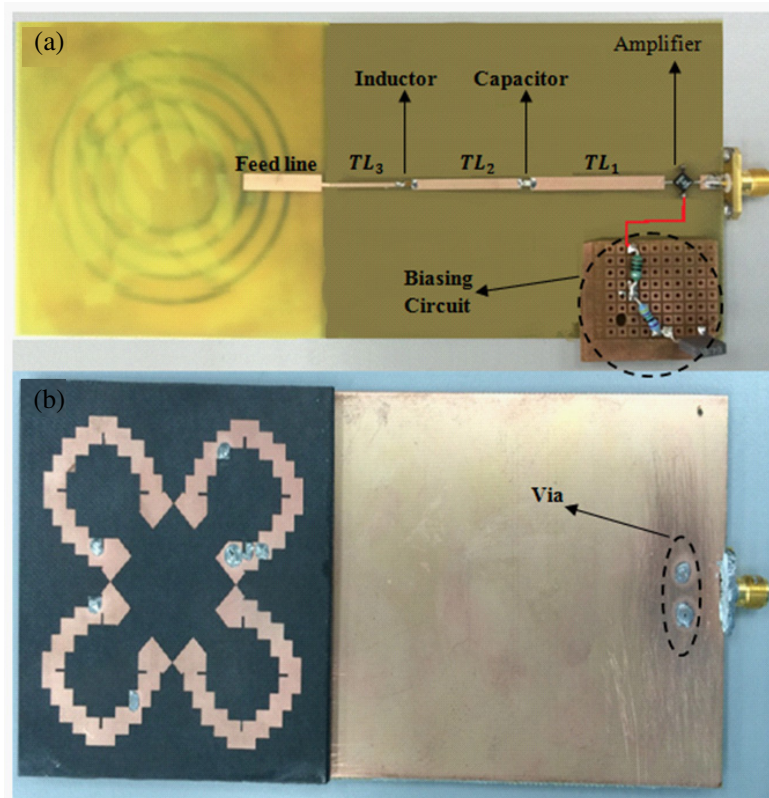


Figure 12. Photograph of the fabricated active antenna. (a) Front view, (b) feeding view and biasing circuit.

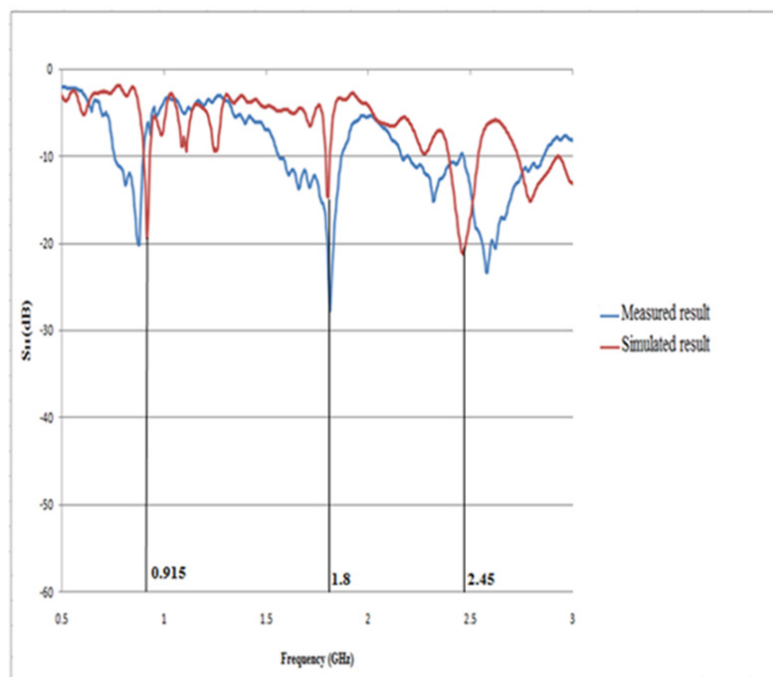


Figure 13. The simulated and measured reflection coefficient results of the proposed active antenna.

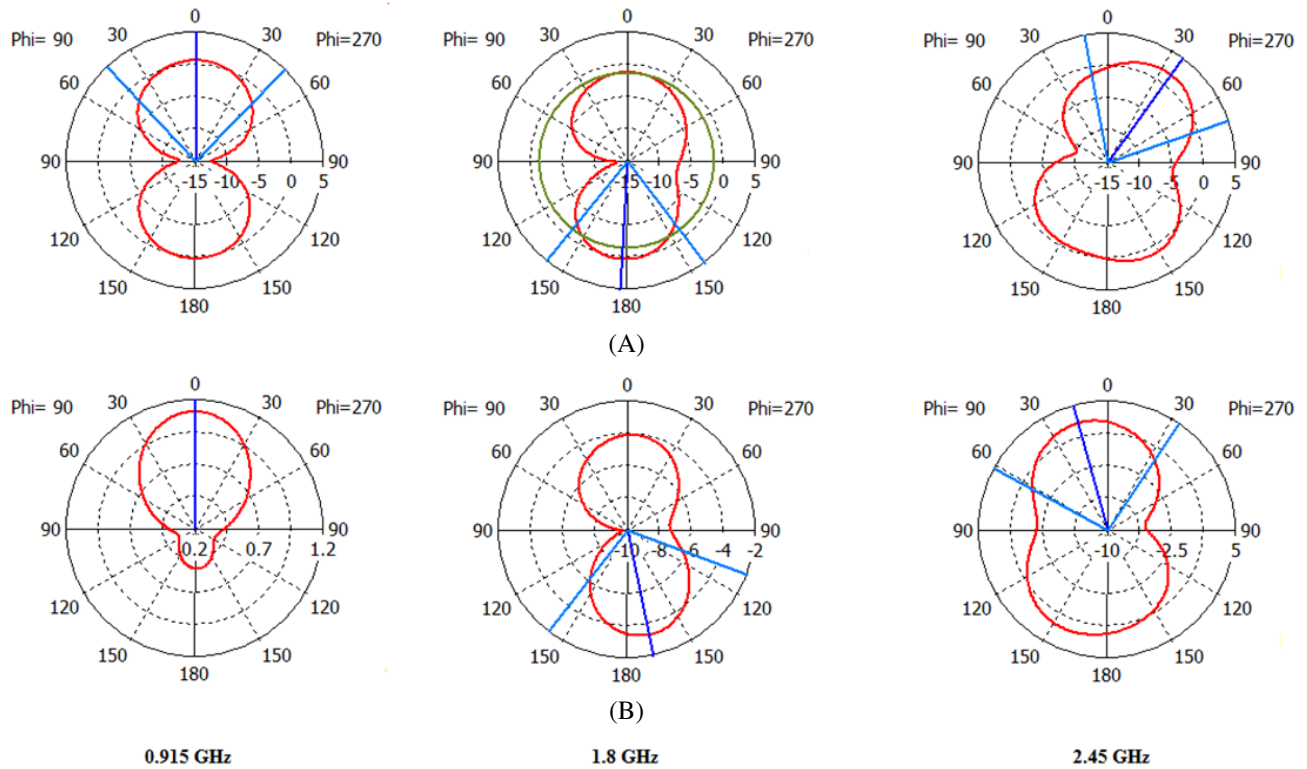


Figure 14. The radiation pattern for the Passive (A) and active antenna (B) at (a) 0.915 GHz, (b) 1.8 GHz and (c) 2.45 GHz.

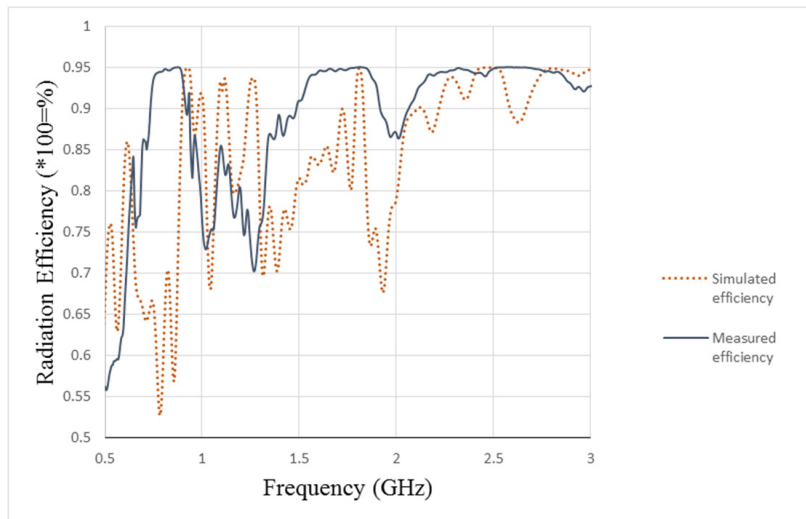
Table 5. Summary of the antenna performance using the four methods.

Methods	f_r (GHz)			
	0.915	1.8	2.45	
Analytical	S_{11}	-18.48	-16.71	-20.43
	Z_{11}	45.43	65.74	47.23
	VSWR	1.27	1.35	1.21
Chebychev	S_{11}	-23.48	-11.54	-16.48
	Z_{11}	41.82	30.79	50.44
	VSWR	1.36	1.73	1.14
PSO	S_{11}	-18.95	-13.4	-16.83
	Z_{11}	41.13	56.82	51.77
	VSWR	1.27	1.55	1.33
GA	S_{11}	-26.95	-21.04	-20.31
	Z_{11}	53.2	43.11	51.2
	VSWR	1.09	1.2	1.2

of the air, the super glue (is used to paste the layers) and fabrication tolerances are removed after matching by the TLT. Besides, Fig. 14 shows a little change in the beamwidth which becomes wider for the active antenna than the passive antenna. In addition, Fig. 15 illustrates a good agreement at the desired resonant frequencies for the measured and simulated radiation efficiencies.

Table 6. The simulated and measured gain.

Frequency (GHz)	Measured gain of the passive antenna in (dB)	Simulated gain of the active antenna in (dB)	Measured gain of the active antenna in (dB)
0.915	0.2	21.75	20.9
1.8	0.512	20.362	19.85
2.45	2.52	21.1	20.88

**Figure 15.** The radiation efficiency of measured and simulated proposed antenna.

5. CONCLUSION

A new concept of high-gain active antenna design using aperture coupled feeding for agriculture application is presented in this paper. Based on the FCC and application requirement, the proposed active antenna is capable of resonating at three different frequencies, 0.915 GHz, 1.8 GHz and 2.45 GHz. A new fractal shape patch by mixing a modified fractal Koch fractal shape and the square loop is applied to achieve a multi-resonance antenna and feasible size reduction. A novel PBG structure is exploited as an aperture in order to remove undesired harmonics and build a stop-band and pass-band. Furthermore, the proposed passive antenna has a miniaturized size almost by 18%, 70%, 30%, 65%, 65%, 12.5%, and 12.5%, respectively. Consequently, the proposed active antenna has a high gain, VSWR less than two, and good radiation efficiency. The results show that the proposed active antenna is a suitable choice for the target application. The measured gains are 20.9 dB, 19.85 dB and 20.88 dB at 0.915 GHz, 1.8 GHz and 2.45 GHz, respectively, which shows a good agreement with the simulated ones.

REFERENCES

1. Watters, F. L., "Microwave radiation for control of tribolium confusum in wheat and flour," *J. Stored Prod. Res.*, Vol. 12, No. 1, 19–25, 1976.
2. Vadivambal, R., "Assessment of microwave energy for disinfestation of grain," No. 05, 2005.
3. Ponomaryova, I. A., L. Nino de Rivera y Oyarzabal, E. Ruiz Sanchez, "Interaction of radio-frequency, high-strength electric fields with harmful insects," *International Microwave Power Institute*, 17–27, Mar. 2010.
4. Esime-culhuacan, S. and I. P. Nacional, "Interaction of radio frequency, high strength electric fields with harmful insects," 17–27, 2003.

5. Nelson, S. O. and P. G. Bartley, "Measuring frequency and temperature dependent permittivities of food materials," *IEEE Transactions on Instrumentation and Measurement*, Vol. 51, No. 4, 589–592, 2002.
6. Garg, R., P. Bhartia, I. Bahl, and A. Ittipibon, *Microstrip Antenna Design Handbook*, *IEEE Antenna and Propagation Magazine*, Vol. 45, No. 2, 875, 2001.
7. Ain, M. F., Y. M. Qasaymeh, Z. A. Ahmad, M. A. Zakariya, and U. Ullah, "An equivalent circuit of microstrip slot coupled rectangular dielectric resonator antenna," *PIERS Proceedings*, 1837–1840, KL, Malaysia, March 27–30, 2012.
8. Waterhouse, R. B., *Printed Antennas for Wireless Communications*, John Wiley Sons Inc., 2007.
9. Ouedraogo, R. O. and E. J. Rothwell, "Metamaterial inspired patch antenna miniaturization technique," *IEEE Antennas and Propagation Society International Symposium*, 1–4, 2010.
10. Sukhadia, M. B. and V. G. Kasabegoudar, "Investigation of mutual coupling effects in conventional and fractal capacitive coupled suspended RMSAs," *International Journal of Wireless Communications and Mobile Computing*, Vol. 1, No. 4, 119–123, 2013.
11. Mandelbrot, B. B., *Fractal and the Geometry of the Nature*, 1st Edition, W. H. Freeman and Company, 1975.
12. Shafie, S. N., I. Adam, and P. J. Soh, "Design and simulation of a modified Minkowski fractal antenna for tri-band application," *Asia International Conference on Mathematical/Analytical Modelling and Computer Simulation (AMS)*, No. 1, 2–5, 2010.
13. Vinoy, K. J., "Fractal shaped antenna elements for wide and multiband wireless applications," The Pennsylvania State University, The Graduate School College of Engineering Fractal, 2002.
14. Salar Rahimi, M. and J. Rashed-Mohassel, "Gain and impedance matching improvement of Sierpinski carpet patch antenna using dual band EBG structure," *Asia-Pacific Microwave Conference Proceedings (APMC)*, 681–684, 2011.
15. Oraizi, H. and S. Hedayati, "Wideband monopole fractal antenna with Hilbert fractal slot patterned ground plane," *2011 41st European Microwave Conference (EuMc)*, 242–245, 2010.
16. Ahmad, B. H., H. Nornikman, M. Z. A. Abd Aziz, M. A. Othman, and A. R. Othman, "Tri-band Minkowski island patch antenna with complementary split ring resonator at the ground plane," *2013 Microwave Technologies Conference*, 46–51, Apr. 2013.
17. Sathya, K., "Size reduction of low frequency microstrip patch antennas with koch fractal slots," M. Tech Thesis, Indian Inst. Sci. Bangalore, 2004.
18. Khare, R. and R. Nema, "Reflection coefficient analysis of Chebyshev impedance matching network using different algorithms," *International Journal of Innovative Research in Science, Engineering and Technology*, Vol. 1, No. 2, 214–218, 2012.
19. Chih-Ming, T., et al., "Nonsynchronous alternating-impedance transformers," *Asia-Pacific Microwave Conference (APMC)*, Vol. 1, 310–313, 2001.
20. Monzon, C., "Analytical derivation of a two-section impedance transformer for a frequency and its first harmonic," *IEEE Microwave and Wireless Components Letters*, Vol. 12, No. 10, 381–382, 2002.
21. Wu, L., et al., "A dual-frequency Wilkinson power divider: For a frequency and its first harmonic," *IEEE Microwave and Wireless Components Letters*, Vol. 15, No. 2, 2004–2006, 2005.
22. José da Silva, H., M. João do Rosario, and C. Peixeiro, "From passive microstrip single patch antennas to active microstrip patch arrays," *Instituto de Telecomunicações*, Lisboa, Portugal, 2001.
23. Lin, J. and T. Itoh, "Active integrated antennas," *IEEE Transactions on Microwave Theory and Techniques*, Vol. 42, No. 12, 1994.
24. Chang, K., R. A. York, P. S. Hall, and T. Itoh, "Active integrated antennas," *IEEE Transactions on Microwave Theory and Techniques*, Vol. 50, No. 3, 937–944, 2002.
25. Swamy, K. and M. Veluri, "Active integrated antenna (AIA) system for wireless communication," *International Journal of Scientific and Research Publications*, Vol. 3, No. 11, 1–5, 2013.
26. Liou, W., et al., "Design and implementation of a low-voltage 2.4-GHz CMOS RF receiver front-end for wireless communication," *Journal of Marine Science and Technology*, Vol. 13, No. 3, 170–175,

- 2005.
27. Pozar, D. M., "Microstrip antennas", *Proceeding of IEEE*, Vol. 80, No. 1, 79–91, 1992.
 28. Peter, T., et al., "Active integrated antenna with low noise amplifier design at 5 GHz," *2nd European Conference on Antennas and Propagation (EuCAP)*, 1–6, Nov. 2007.
 29. Zurcher, J. F. and F. E. Gardiol, *Broadband Patch Antennas*, Artech House, Norwood, MA, 1995.
 30. Radisic, V., et al., "Novel 2-D photonic band gap structures for microstrip lines," *IEEE Microwave Guided Wave Lett.*, Vol. 8, 69–71, 1998.
 31. Qian, Y., et al., "Microstrip patch antenna using novel photonic band gap structures," *Microwave J.*, Vol. 42, 66–76, Jan. 1999.
 32. Karmakar, N. C. and M. N. Mollah, "Investigations into nonuniform photonic-bandgap microstripline low-pass filters," Vol. 51, No. 2, 564–572, 2003.
 33. [Http://www.minicircuits.com/MCLStore/ModelInfoDisplay?14093539187760.14037500767787614](http://www.minicircuits.com/MCLStore/ModelInfoDisplay?14093539187760.14037500767787614), "Surface mount amplifier," *Mini Circuit*.
 34. Khodier, M., et al., "Design of multiband multi-section transmission line transformer using particle swarm optimization," *Electrical Engineering*, Springer, Vol. 90, No. 4, 293–300, 2008.
 35. Pozar, D. M., *Microwave Engineering*, Addison-Wesley Publ. Co., 1993.
 36. Orfanidis, S. J., "A two-section dual-band Chebyshev," *IEEE Microwave and Wireless Components Letters*, Vol. 13, No. 9, 382–384, 2003.
 37. Ming, C., "Novel design method of a multi-section transmission-line transformer using genetic algorithm techniques," *International Conference on Electrical Machines and Systems (ICEMS)*, 3793–3796, 2008.
 38. Coupler, D., *Antenna Measurements*, IEEE Library, 120–129.
 39. Noori, O., J. Chebil, M. R. Islam, and S. Khan, "Design of a triple-band h slot patch antenna," *International Conference on RF and Microwave (RFM)*, 289–292, Dec. 2011.
 40. Kulkarni, S. D. and S. N. Makarov, "A compact dual-band foam-based UHF PIFA," *IEEE Antennas and Propagation Society Symposium*, 3609–3612, 2006.
 41. Ávila-navarro, E., J. A. Carrasco, and C. Reig, "Dual printed antenna for Wi-Fi applications," *IEEE Antennas and Wireless Propagation Letters*, Vol. 8, 596–598, 2009.
 42. Dai, X.-W., Z.-Y. Wang, X. Chen, and L. Wang, "Multiband and dual-polarized omnidirectional antenna for 2G/3G/LTE application," *IEEE Antennas and Wireless Propagation Letters*, Vol. 12, 1492–1495, 2013.
 43. Kim, S. and K. Min, "Design for multiband monopole antenna with parasitic elements for in-building mobile communication," *Wireless and Mobile*, 92–95, 2014.
 44. Sharma, D. and M. S. Hashmi, "A novel design of tri-band patch antenna for GSM/WiFi/WiMAX applications," *Microwave and RF IEEE International Conference (IMaRC)*, 156–158, 2014.
 45. Rouissi, I., I. B. E. N. Trad, J. F. H, H. Rmili, and H. Trabelsi, "Design of frequency reconfigurable triband antenna using capacitive loading for wireless communications," *Antennas & Propagation Loughborough Conference (LAPC)*, 3–7, 2015.